PECULIARITIES OF NUCLEATION AND ORDERING OF GeSi NANOISLANDS IN MULTILAYER STRUCTURES FORMED ON Si AND $Si_{1-x}Ge_x$ BUFFER LAYERS

V.O. YUKHYMCHUK,[1] M.YA. VALAKH,[1] V.P. KLADKO,[1] M.V. SLOBODIAN,[1] O.YO. GUDYMENKO,[1] Z.F. KRASILNIK,[2] A.V. NOVIKOV[2]

[1]V. Lashkaryov Institute of Semiconductor Physics, Nat. Acad. of Sci. of Ukraine
(41, Prosp. Nauky, Kyiv 03028, Ukraine; e-mail: kladko@isp.kiev.ua)

[2]Institute for Physics of Microstructures, Russian Academy of Sciences
(GSP-105, Nizhnii Novgorod 603600, Russia)

PACS 61.05.cp, 64.75.Qr, 68.55.ag, 68.65.Hb, 78.55.Ap, 81.07.Ta

High resolution X-ray diffraction (HRXRD), Raman scattering (RS), and photoluminescence (PL) methods have been used to study the influence of $Si_{1-x}Ge_x$ buffer layer parameters on the spatial ordering of self-assembled Ge nanoislands in multilayer SiGe/Si structures grown on Si (001) substrates. The thickness and the composition of a $Si_{1-x}Ge_x$ buffer layer are shown to affect the lateral ordering of nanoislands owing to the different sensitivities to the ordered strain modulation in the layer surface. The spatial ordering is found to be governed exclusively by the lateral ordering in the first period of the superlattice (SL). It is demonstrated that, in the case of thick $Si_{1-x}Ge_x$ buffer layers with a considerable Ge content, a plastic relaxation is accompanied by the emergence of mismatch dislocations at the interface, when the SL layers are coherent to the buffer one. The complex researches of the corresponding structural and optical characteristics allow us to develop methodological approaches to the study of the nanoisland ordering in the SL.

1. Introduction

Application of structures with self-assembled Ge/Si nanoislands opens new prospects for the development of opto- and nanoelectronics [1]. Arrays of Ge (GeSi) quantum dots (QDs) can be successfully used to manufacture photodetectors and light-emitting diodes in the near infra-red range, because they possess certain advantages over traditional Ge/Si structures with quantum wells [2]. There are a number of factors favorable for the application of multilayer structures with Ge QDs in new-generation thermoelectric devices [3]. Germanium QDs are among potential candidates to be implemented in quantum computers [4]. The manufacture of multilayer arrays of Ge QDs in Si matrices is promising from the viewpoint of their application to solar cells and other devices [5].

However, the wide application of Si/Ge nanoislands in opto- and nanoelectronics can become really possible, only if the parameters of grown structures can be exactly predicted and controlled at the quantitative level. Such parameters of nanoislands as their shape, dimensions, composition content, mechanical stresses, and surface concentration depend in a complicated manner on growing conditions. Ge/Si islands can have the shapes of hut clusters, pyramids, domes and superdomes which can change their shape when growing silicon over them. In most cases, multilayer structures – SLs with nanoislands formed in every layer – are grown for operating electronic devices. This allows the total number of active elements, which can play the role of emitters, absorption detectors, and so forth, to be increased. On the other hand, the growing of multilayer structures with nanoislands allows one to control parameters of the latter within certain ranges owing to the influence of already formed islands on those which are being formed. As a result, the vertical and lateral ordering of nanoislands can be substantially enhanced.

Traditionally, SLs with Ge (GeSi) nanoislands are grown on Si buffer layers. For nanoislands in a SL, typical is a manifestation of ordering along the direction of growth, the so-called vertical correlation [6]. At the same time, the formation of nanoislands on $Si_{1-x}Ge_x$ buffer layers (with low x-values) is known to result in their partial lateral ordering [7]. Therefore, the usage of $Si_{1-x}Ge_x$ buffer layers to form ordered nanoislands should facilitate the enhancement of their ordering in the SL bulk. Two major scenarios can be considered. In the first one, only one $Si_{1-x}Ge_x$ buffer layer, which sets the ordering of nanoislands throughout the whole SL, is used. In the second, a $Si_{1-x}Ge_x$ buffer is formed for every SL period.

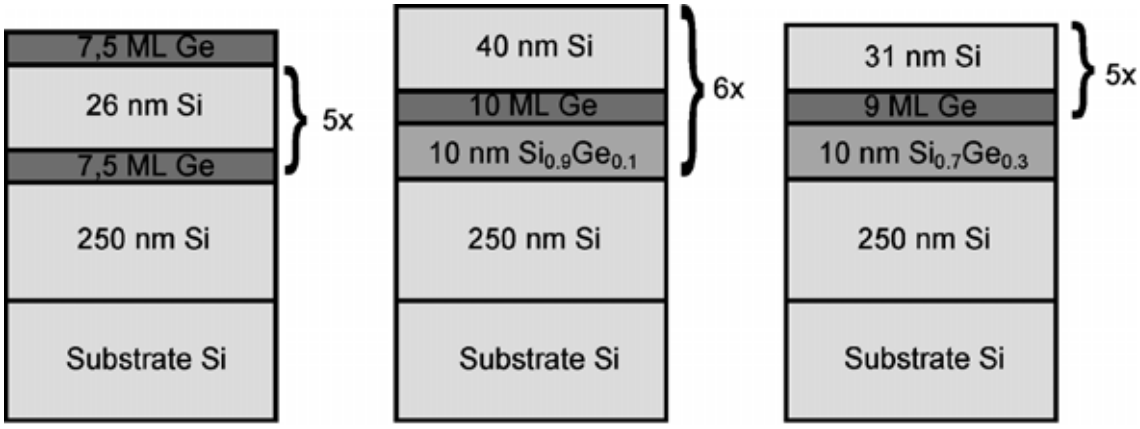

a **b** **c**

Fig. 1. Schematic diagrams of examined structures 1 (*a*), 2 (*b*), and 3 (*c*)

This work is aimed at determining the ordering parameters and features of GeSi nanoislands formed in a SL with the use of $Si_{1-x}Ge_x$ and Si buffer layers of various types, as well as their dependences on the thickness of SL structure layers.

2. Experimental Technique

Multilayer structures were produced using the method of molecular beam epitaxy (MBE) of Ge and Si onto a Si (001) substrate with a preliminarily grown silicon buffer layer 250 nm in thickness. Three types of the multilayer structures obtained at a temperature of 600 °C were studied. Structure 1 was formed by depositing 7.5 ML of Ge onto a silicon layer; afterwards, the formed islands were covered with a silicon layer 26 nm in thickness. This procedure was repeated five times. The upper layer of islands was not covered with silicon. The structure of this type is schematically exhibited in Fig. 1,*a*, and the corresponding transmission electron microscopy (TEM) image is depicted in Fig. 2. Structure 2 was fabricated by depositing 6 periods of the following sequence of layers: 10-nm $Si_{0.9}Ge_{0.1}Si$/10-ML Ge/40-nm Si (Fig. 1,*b*). Structure 3 was formed by depositing 9 ML of Ge onto a preliminarily grown 10-nm $Si_{0.7}Ge_{0.3}$ layer; afterwards, the formed islands were covered with a silicon layer 31 nm in thickness; the procedure was repeated five times (Fig. 1,*c*).

The RS spectra were registered at room temperature on a DFS-24 double diffraction spectrometer. The spectra were excited by Ar-laser irradiation at a wavelength of 487.9 nm. The signal was registered using a Hamamatsu-R2949 cooled photoelectronic multiplier operating in the photon-count mode. The experiments

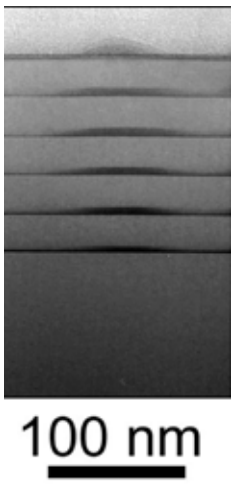

Fig. 2. TEM image of a multilayer structure with $Si_{1-x}Ge_x$ nanoislands formed at a temperature of 600 °C. The nominal thicknesses of Ge and Si layers are 7.5 ML and 26 nm, respectively

were carried out in the "backscattering" geometry. For the positions of RS bands to be determined more precisely, the plasma lines of an Ar-laser with well-known frequencies were used as reference marks. The PL spectra were registered on a BOMEM DA3.36 Fourier spectrometer at a temperature of 77 K. The spectra were excited by Ar-laser irradiation at a wavelength of 514.5 nm.

For all fabricated SLs, we measured the diffraction reflection curves (DRC) for 004 symmetric and 224 asymmetric reflections on a PANalytical X'Pert Pro MRD XL high-resolution diffractometer with a 4-fold Ge (220) monochromator and a 3-fold analyzer of the same type. Specimens were scanned in a vicinity of their exact Bragg position in the ω- and $(\omega - 2\theta)$-scanning modes. Two-dimensional maps of scattered intensity distributions

around sites 004, 113, and 224 of the reciprocal lattice were recorded. The thickness of SL layers was determined from the DRC oscillations in the Bragg geometry. The SL structural parameters were corrected by simulating the diffraction spectra [8, 9] and carrying out a subsequent autofitting procedure [10, 11].

3. Results and Discussion

The so-called vertical correlation is typical of nanoislands in multilayer structures. As can be seen from Fig. 2 for structure 1, every island in the upper layer is located just above an island in the lower layer. Such an arrangement of islands is connected with the influence of strain fields created by islands located in the lower layers. If the thickness of a silicon spacer does not exceed 100 nm and the island heights are about 5 nm and more, the stress fields are transferred coherently to the next Ge layer [6]. As a result, Ge islands are formed at those sites in the upper layer, where the tensile stresses in the Si spacer are maximal. In work [12], we demonstrated that the island formation on a Si layer with tensile stresses differs from the standard situation. In the course of Ge epitaxy onto such a silicon layer, the available stresses give rise to a transformation from the layer-by-layer growth regime to the island one at thinner thicknesses of the wetting Ge layer. In this case, more Ge atoms that are deposited during MBE take place in the formation of islands, and, respectively, the islands are bigger. To obtain islands with identical dimensions over the whole SL, tne number of deposited Ge monolayers must be less by one starting from the second layer.

3.1. RS researches

The characteristic feature of multilayer structures with nanoislands consists in that a new periodicity different from that of initial substances is realized. This periodicity gives rise to a "convergence" of the dispersion branch of acoustic phonons and to the manifestation of acoustic phonons in the spectral range typical of the optical ones. Concerning to optical photons, the asymmetric bands with low-frequency shoulders are observed in RS spectra at room temperature, which are caused by an insignificant slope of the dispersion branch for Si and Ge in the interval from $k = 0$ to $k = \pi/a$ of the Brillouin zone, where a is the crystal lattice parameter.

It should be noted that, in the course of RS spectrum registration for multilayer structures, we obtain the parameter values that are averaged over all islands in the examined structure, which are located down to the depth $d \approx 1/2\alpha$, where α is the effective absorption coefficient. Owing to a spread of the composition content in islands, which brings about a spread of elastic strain magnitudes, the RS bands reveal a considerable broadening.

In the SL with nanoislands, the effective volume of islands that contribute to the light scattering is small in comparison with the volumes of the silicon matrix and the substrate part. In the case of a short-period SL and a small thickness of its layers, a large contribution to the RS signal is given by the Si substrate; in the case of a long-period SL, such contributors are silicon spacers. In the experimental spectrum, this contribution manifests itself in the form of an intense silicon-induced band at a frequency of about 520 cm^{-1} which can overlap the band induced by the Si–Si mode in the islands. In addition, the 2TA mode with a frequency of about 300 cm^{-1} induced by silicon spacers and the substrate can overlap the Ge–Ge mode given by SiGe nanoislands. For the positions of RS bands that correspond to atomic vibrations in islands to be determined exactly, we subtracted the RS spectrum of the silicon substrate from the spectrum given by the island structure, both being registered under identical conditions. In work [13], we showed that MBE at a temperature of 600 °C is accompanied by a huge Si diffusion from the substrate and spacers onto islands, the phenomenon being connected with inhomogeneous stresses around the latter. As a result, the islands are a solid SiGe solution characterized by three dominant modes in the RS spectrum.

Note that, for the correct determination of island composition content x and the elastic strain ε to be correct, we consider the influence of every possible factor on the positions of RS bands. According to the atomic force microscopy [13] and TEM studies, the islands formed at the temperature $T_p \geq 600$ °C have an average height of 4–5 nm and the lateral dimensions of about 70 nm. Therefore, the influence of size confinement on the phonon frequency can be neglected in our case. Hence, the positions of RS bands induced by SiGe nanoislands are governed by their composition content and the elastic strain magnitude. As for the intensities of the Ge–Ge and Ge–Si bands, they depend on the nominal amount of deposited Ge and the closeness between the exciting laser radiation energy and the energy of optical transitions in nanoislands.

Figure 3 illustrates the RS spectra of three studied structures. It is evident that the intensities of bands produced by structure 3 are substantially lower than the corresponding values in two other cases. The nominal thicknesses of deposited Ge layers do not differ substantially for all three structures (ranging from 7.5 to

10 ML). This means that the conditions for the RS intensity amplification favored by the resonance were not satisfied for specimen 3. Such considerable differences in the RS spectra can be associated with the fact that islands were not formed in structure 3, or they have dimensions that considerably differ from those in structures 1 and 2. This result turned out a little unexpected. We showed that nanoislands that are formed on $Si_{1-x}Ge_x$ buffer layers ($0.1 \leq x \leq 0.25$) have larger average dimensions than those grown on the Si buffer [7], because the number of Ge atoms that participate in the island formation increases due to a reduction of the thickness of the wetting layer on the $Si_{1-x}Ge_x$ buffer at the 2D–3D transition. Islands could not be formed on the $Si_{0.7}Ge_{0.3}$ buffer layer, owing to the emergence of mismatch dislocations (MDs) and their intergrowth into all upper layers of the SL. In this case, first, the elastic energy of the buffer layer decreases, and, second, the average value of lattice parameter in the $Si_{0.7}Ge_{0.3}$ buffer layer grows. Both phenomena result in an increase of the nominal thickness of the Ge layer, at which the 2D–3D transition takes place. Therefore, nine deposited monolayers of germanium might turn out insufficient to invoke the island formation. Additional information concerning the island formation can be extracted from PL and HRXRD spectra, which will be discussed below. By analyzing the frequency positions of RS bands in the spectra of two other structures, we can estimate the composition content and the elastic strain. Note that two Ge–Si bands are observed in the RS spectrum of specimen 2: they correspond to Ge–Si vibrations in islands and in $Si_{1-x}Ge_x$ buffer layers, respectively.

The frequency of each mode in a $Si_{1-x}Ge_x$ solid solution is known to depend on the composition content x and the elastic strain ε as follows [14, 15]:

$$\omega_{\mathrm{SiSi}} = 520,5 - 62x - 815\varepsilon, \quad (1)$$

$$\omega_{\mathrm{GeSi}} = 387 + 81(1-x) - 78(1-x)^2 - 575\varepsilon, \quad (2)$$

$$\omega_{\mathrm{GeGe}} = 282.5 + 16x - 385\varepsilon. \quad (3)$$

Composition and elastic strain of islands in multilayer structures

Specimen No	Ge content in islands, x	Elastic strain (ε), (according to RS results)	Elastic strain (ε), (according to HRXRD results)
1	0.65 ± 0.04	-1.6 ± 0.3	-1.3 ± 0.2
2	0.75 ± 0.02	-1.0 ± 0.2	-1.1 ± 0.1
3	No islands were formed		

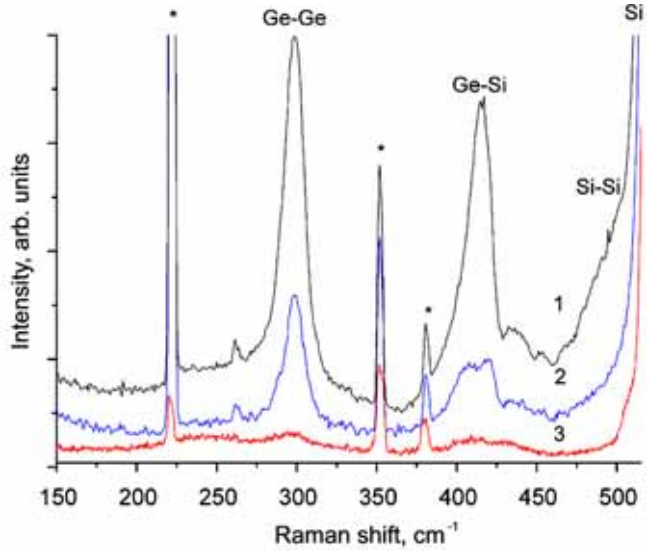

Fig. 3. Experimental RS spectra of structures grown at 600 °C. Asterisks mark the bands that correspond to plasma discharges in an Ar^+-laser

Substituting the frequencies of Ge-Ge, Ge–Si, and Si–Si vibrations determined from experimental spectra and solving the system of equations (1)–(3) graphically, as was shown in work [1], we calculated the x- and ε-values, which are given in the Table. The data obtained testify that the silicon content in the islands formed on $Si_{1-x}Ge_x$ buffer layers (specimen 2) is a little lower in comparison with that in the islands formed on Si layers (specimen 1).

3.2. Photoluminescence

It is known that Si and Ge are indirect band-gap semiconductors, so that the emission efficiency of bulk structures fabricated on the basis of those substances is very low. To obtain SiGe-based structures which would emit in the near IR range, it is necessary to create a SiGe quantum well (quantum dots), where current carriers would be localized. For this purpose, the silicon layer is grown above SiGe islands in the course of epitaxy. The GeSi/Si heterostructures created in such a manner are referred to type II. This type of heterostructures is characterized by breaks in the conduction and valence bands at the heterostructure interface [16]. The breaks are arranged in such a manner that the potential well for holes is located in $Si_{1-x}Ge_x$ islands and that for electrons in the silicon matrix. The elastic deformation of compression in $Si_{1-x}Ge_x$ islands results in the elimination of a degeneration in six equivalent Δ-valleys in the conduction band.

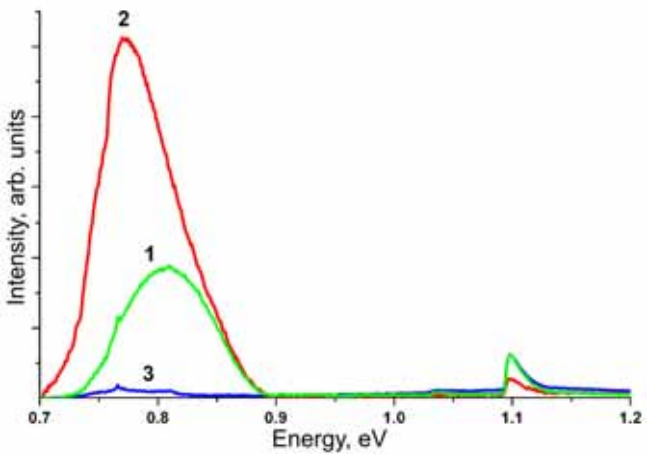

Fig. 4. PL spectra registered for structures 1 to 3 at a temperature of 77 K

The conduction band bottom is formed by twice-degenerate 2Δ-valleys which are prolate in the direction of $Si_{1-x}Ge_x$ growth. The conduction band of silicon is shifted in the same direction, but in the momentum space, with respect to the valence band top in $Si_{1-x}Ge_x$ islands. It follows from the uncertainty relation that the quasimomenta of those electrons in the Si matrix, which are localized near the heterointerface, can be arbitrary in the indicated direction of band shift, including the case $k = 0$. That is, the probability of a direct, in the momentum space, interband electron transition from the conduction band of silicon into the valence band of $Si_{1-x}Ge_x$ islands by means of tunneling in the real space through the heterointerface becomes different from zero. Holes from the surrounding silicon matrix are accumulated in the potential wells—nanoislands—charging them positively. Owing to the Coulomb repulsion in nanoislands, the holes are concentrated along the heterointerface with the silicon matrix. The positive charge of islands gives rise to a bend of the conduction band bottom in silicon and creates a quantum well for electrons in silicon near the heterojunction. In that way, there emerges a possibility for quasidirect band-gap radiative recombination between electrons in silicon and holes in nanoislands. To increase the emission intensity, the structures with nanoislands should be grown as multilayer ones.

The PL spectra for our structures, which were obtained at a temperature of 77 K, are depicted in Fig. 4. One can see that, for specimens 1 and 2, a PL band typical of SiGe nanoislands emerges in the range $0.7-0.9$ eV [16], whereas this band is absent in the PL spectrum of specimen 3. This fact can testify that no nanoislands were formed in the latter structure. The low-intensity PL band for this structure with a maximum at 0.81 eV may correspond to the dislocation band D_1 [17]. Even an insignificant dislocation concentration can result in another scenario of the stress relaxation in the $Si_{0.7}Ge_{0.3}/Ge/Si$ system.

3.3. X-ray diffraction researches

The macroscopic relaxation of stresses in and the composition content of the examined structures were estimated within the HRXRD method. The ω- and $(\omega-2\theta)$-scanning, as well as the reciprocal space maps (RSM) around sites 004 and 113, were used. In order to determine the composition content of and the stresses in SiGe using the method of X-ray diffraction, we used the following formalism. Let us suppose that the SiGe layer, when deposited onto a silicon (001) substrate, is tetragonally distorted. Then, the nondistorted lattice parameter in the SiGe layer, a_{SiGe}, is connected with the lattice parameters in the growth plane, $a^{\parallel}_{\mathrm{SiGe}}$, and perpendicularly to it, $a^{\perp}_{\mathrm{SiGe}}$, by the relation

$$a_{\mathrm{SiGe}} = \left[(1-\nu)/(1+\nu)\right] a^{\perp}_{\mathrm{SiGe}} + \left[2\nu/(1+\nu)\right] a^{\parallel}_{\mathrm{SiGe}}, \quad (4)$$

where ν is Poisson's ratio. For calculations, the dependence of the nondistorted SiGe lattice parameter on the Ge content x was taken in the form [6]

$$a(x) = 5.4309 + 0.20032x + 0.026274x^2 \ (\text{Å}). \quad (5)$$

The degree of stress relaxation R can be presented as the ratio

$$R = \left(a^{\parallel}_{\mathrm{SiGe}} - a_{\mathrm{Si}}\right) / \left(a_{\mathrm{SiGe}} - a_{\mathrm{Si}}\right). \quad (6)$$

Therefore, the precise determination of the Ge content x and the degree of stress relaxation R requires knowing the results of SiGe lattice parameter measurements both along the growth direction and perpendicularly to it. The lattice parameter $a^{\perp}_{\mathrm{SiGe}}$ can be determined using the Bragg law

$$a^{\perp}_{\mathrm{SiGe}} = \frac{2\lambda}{\sin\left(\theta^{\mathrm{Si}}_{004} + \Delta\omega_{004}\right)}, \quad (7)$$

where λ is the wavelength, and $\Delta\omega_{004}$ is the angular distance between the peak given by the substrate and the maximum of satellite-peak envelope which is determined by the Ge content in SiGe layers at the $(\omega-2\theta)$-scanning around diffraction site 004, and $\theta^{\mathrm{Si}}_{004}$ is the Bragg angle for the 004 silicon reflection.

Respectively, the lateral lattice parameter $a^{\parallel}_{\mathrm{SiGe}}$ is calculated by the formula

$$a^{\parallel}_{\mathrm{SiGe}} = \frac{\sqrt{2}\lambda}{\sqrt{\left(a^{\perp}_{\mathrm{SiGe}}\right)^2 \sin^2\left(\theta^{\mathrm{Si}}_{224} + \Delta\omega_{224}\right) - 4\lambda^2}}\, a^{\perp}_{\mathrm{SiGe}}. \quad (8)$$

To compensate substrate misorientations, we used the lattice parameter value averaged over the scans in [110], [1–10], [−1–10], and [−110] diffraction plane directions [18].

Figure 5 exhibits the $(\omega - 2\theta)$-scans for all three structures together with the corresponding fitting spectra. One can see that the fitting DRCs agree rather well with the experimental ones. Near the peak connected with the substrate (Si), we observe the fundamental peak associated with the SL–the so-called zero-order satellite dependent on the lattice parameter averaged over the SL period–and the satellites of higher orders. In all DRCs, the satellite peaks up to the tenth order can be observed, which evidences a high-quality interface between the layers and an insignificant dispersion of SL periods. The SL period T is determined in terms of the distance between neighbor satellites [10, 11] as follows:

$$T = \frac{|\gamma_h|\,\lambda}{\sin\left(2\theta_{\mathrm{B}}\right)\delta\theta}, \quad (9)$$

where $\delta\theta$ is the angular distance between satellites, θ_{B} the Bragg angle, and γ_h the direction cosine.

The lattice parameter averaged over the SL period, $\langle d\rangle$, is determined using the angular distance $\Delta\theta$ between the peak given by the substrate and the zero-order satellite:

$$\varepsilon_{\mathrm{aver}} = \frac{\langle d\rangle - d_0}{d_0} = -\frac{\Delta\theta}{\tan\left(\theta_{\mathrm{B}}\right)\frac{2|\gamma_h|}{\gamma_0+\gamma_h}}, \quad (10)$$

where d_0 is the distance between Si (004) planes, and γ_0 and γ_h are the direction cosines of the primary and diffracted waves at the Bragg maximum with respect to the inner normal to the surface.

The shift of the interference-peak envelope toward smaller angles for specimen 3 corresponds to the position and the shape of a diffraction maximum produced by the $Si_{0.7}Ge_{0.3}$ buffer layer which lies under the grown SL. Scattering by this layer modulates the diffraction image of scattering by the periodic SL structure. From Fig. 5, one can see that there is a split of coherent SL satellites in the spectrum of specimen 2. This phenomenon can result from the presence of two different SL periods along the growth axis, i.e. in the [001] direction or/and the presence of regions located in the SL and oriented

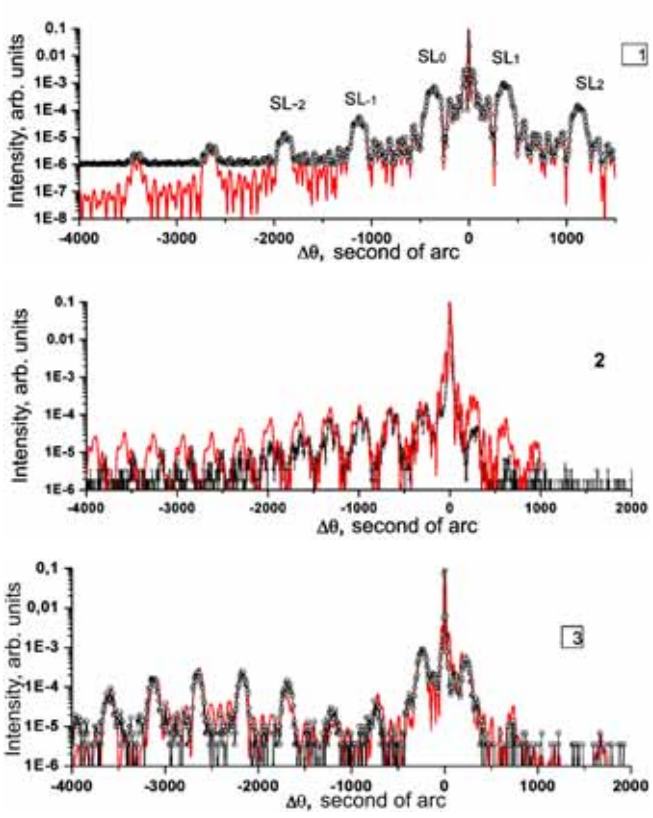

Fig. 5. Triple-axis $(\omega - 2\theta)$-curves of diffraction reflection for reflection 004 of studied structures 1 to 3: experiment (solid curve), fitting curve (circles)

along the growth direction with different characteristic values of germanium content in the layers. The second reason is more probable, because the values of split periods practically coincide with each other. Two systems of peaks-satellites are shifted by an angular distance of about $80 - 120''$. Such a magnitude corresponds to a variation of the germanium content by $\Delta x \approx 0.7 \pm 0.1$. The peak shapes can be used to determine the Ge content changes along the vertical direction in the multilayer structure. The broadening of SL peaks in the $(\omega - 2\theta)$-scan registered in the direction normal to the reflection planes is $\delta\theta_0 = 55''$. The uniform broadening of SL peaks does not depend on their order and can be connected with a variation δx of the average Ge content in the islands along the SL growth direction. This variation of the Ge content can be estimated from the difference $(\Delta\theta_0 = -355'')$ between the angular positions of the SL zero-peak, which corresponds to the Bragg peak of SiGe layers with the same average Ge content, and the

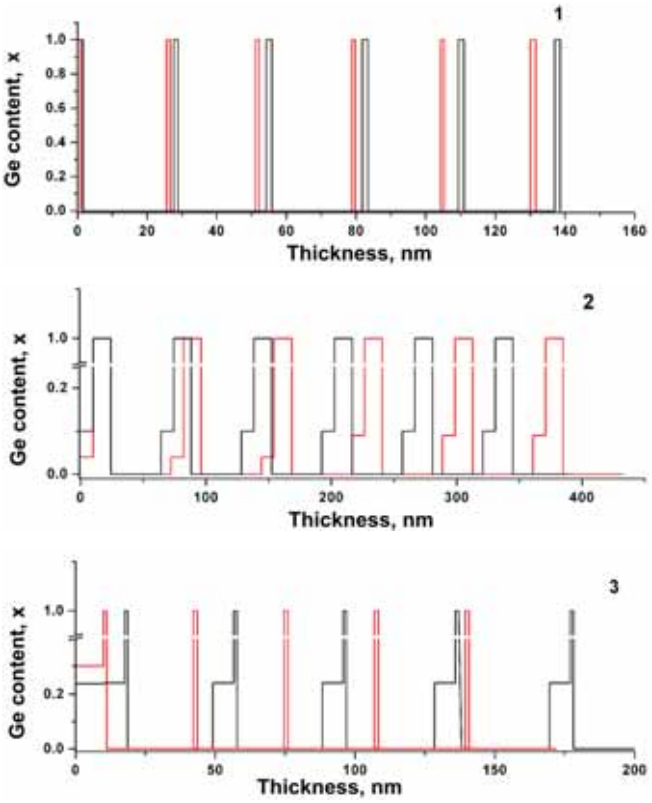

Fig. 6. Variations of the germanium content along the SL depth: fitting curve (black), technologically given parameters (red)

Si (004) peak:

$$\delta\langle x\rangle = \frac{\delta\theta_0}{\Delta\theta_0} = \frac{55}{355} = 15.5\%. \qquad (11)$$

The distribution of the Ge content and its variation over the depth of SL structures, which were obtained using the fitting procedure, are depicted in Fig. 6. The analysis of plots given in this figure demonstrates that the experimental and the technologically given distributions of the Ge content over the structure thickness are in qualitative agreement with each other for specimen 1. Certain differences in the thicknesses stem from the fact that some part of Ge was spent on the formation of nanoislands. Concerning the dependence of the Ge content on the thickness for specimen 2, we may assert that it confirms what was said above about the existence of two regions with different germanium contents. It is this circumstance that is responsible for the presence of two different SL periods along the [001] direction. At last, the largest discrepancies between the technological and experimental Ge distributions in the SL layers are observed for specimen 3. They can originate from the largest degree of relaxation of this structure, which gives rise to the germanium redistribution over layers.

For the determination of the relaxation degree in the systems, we measured and analyzed the maps of intensity distributions around the reciprocal lattice sites. The corresponding maps are presented in Fig. 7 for both symmetric, 004, and asymmetric, 113, reflections. As follows from the RSMs, all the structures are coherent with respect to the substrate and the buffer layers (the system of peaks-satellites is arranged along the growth axis).

The RSM analysis showed that no islands were formed in specimen 3. This follows from the absence of the typical diffusive background around the system of coherent satellites given by the SL. This result is to some extent unexpected, because the nominal thickness of deposited germanium exceeds the critical value. The critical thickness of Ge deposited at $T = 600$ °C onto a silicon buffer–i.e. the thickness of Ge layer, at which the 2D–3D transition takes place—amounts to 4 ML. In the case of $Si_{1-x}Ge_x$ buffer layers, the critical thickness decreases with the growth of x [19]. However, the mechanism of stress relaxation can be different from the classical Stranski–Krastanov one. Namely, it occurs through the formation of mismatch dislocations (MDs). The MD concentration can be insufficient for the dislocations to be revealed using experimental methods. Nevertheless, they bring about the relaxation in a buffer layer, as well as in the whole structure, so that nanoislands are not formed or are formed at different thicknesses of deposited germanium. In specimens 2 and 1, we observe the scattering by a system of nanoislands. However, only the last system turns out well-ordered in the growth plane, because the asymmetric map for the 113 reflection demonstrates pronounced lateral satellites in a vicinity of the coherent zero-order satellite. The lateral satellites are diffraction maxima of resonance diffusion scattering. The distance between them in the reciprocal space, by analogy with the distance between coherent satellites, corresponds to the reciprocal value of the lateral SL period. For specimen 1, the latter equals 240 nm.

In specimen 2, nanoislands are only at the initial stage of their lateral ordering. The corresponding lateral period is 229 ± 3 nm. The lateral ordering of islands in this structure is worse in comparison with that in specimen 1, because the separating silicon layer in this SL is thicker. As a consequence, nanoislands in every next wetting layer feel the influence of the strain fields induced by nanoislands in the previous layers more weakly. In other words, the so-called vertical correlation is absent. Moreover, every SL period includes a $Si_{0.9}Ge_{0.1}$ layer

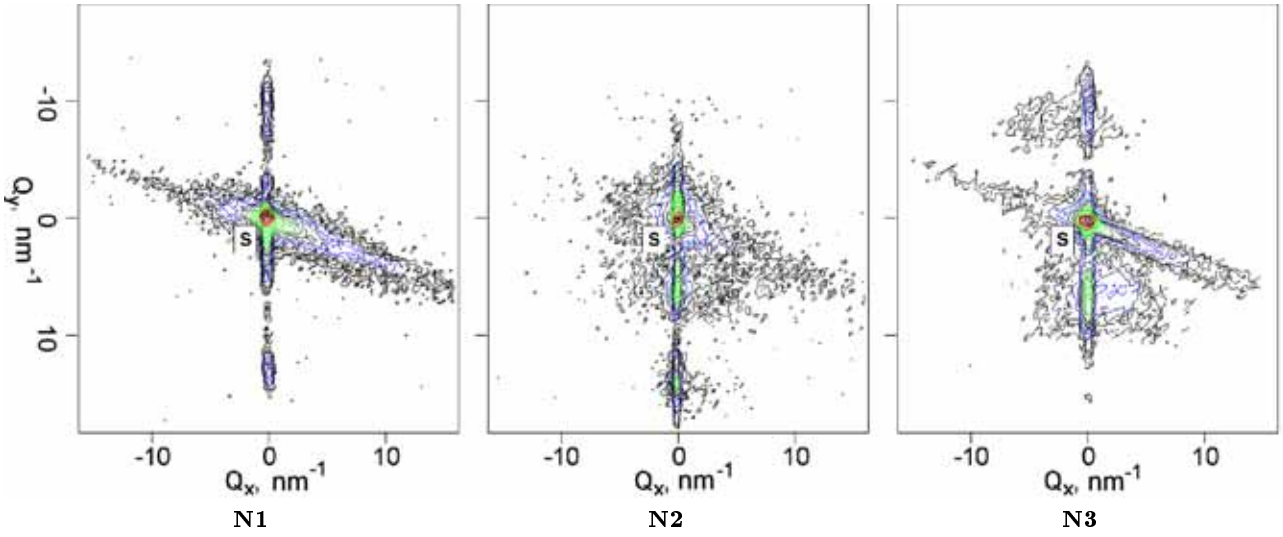

Fig. 7. 113 reciprocal space maps for specimens 1 to 3

which also reduces the influence of strain fields penetrating from below.

It is necessary to note that, for all specimens, the diffusion background appears in the ω-scans (to the left from the fundamental peak) and in the RSMs (perpendicularly to the diffraction vector). This diffusion background is stimulated by the dislocation structure (mainly, the MDs) at the silicon–buffer layer interface.

4. Conclusions

Hence, on the basis of the results of our researches obtained using the high-resolution x-ray diffraction, Raman light scattering, and photoluminescence methods and dealing with peculiarities of the spatial ordering of self-assembled GeSi nanoislands in multilayer SiGe/Si structures, the following conclusions can be drawn:

1) the thickness of a separating silicon layer in the SL period affects the spatial formation of the ordered system of SiGe nanoislands;

2) the thickness and the composition content of a buffer layer affects the lateral ordering of nanoislands owing to the different sensitivity to the ordered strain modulation on the layer surface;

3) the spatial ordering of nanoislands is governed exclusively by the lateral ordering in the first SL period;

4) in the case of thick buffer layers, a plastic relaxation begins; it is accompanied by the emergence of mismatch dislocations at the buffer layer–substrate interface, and the SL layers are coherent to the buffer layer;

5) a new methodological approach has been proposed to study the nanoisland ordering in multilayer structures, as well as their key parameters.

This work was sponsored in the framework of following projects: project 3.5.1.12/19 of the State goal-oriented scientific and technological program "Nanotechnologies and nanomaterials" (National Academy of Sciences of Ukraine), project M90/2010 (Ministry of Education and Science of Ukraine), and project 32-08-10-Ukr (Programs of collective researches, National Academy of Sciences of Ukraine and Russian Fund for Fundamental Researches).

1. K. Brunner, Rep. Prog. Phys. **65**, 27 (2002).
2. S. Tong, J. Liu, L.J. Wan, and K.L. Wang, Appl. Phys. Lett. **80**, 1189 (2002).
3. L.D. Hicks and M.S. Dresselhaus, Phys. Rev. B **47**, 12727 (1993).
4. R. Vrijen, E. Yablonovitch, K. Wang, H.W. Jiang, A. Balandin, V. Roychowdhury, T. Mor, and D. Di Vincenzo, Phys. Rev. A **62**, 012306 (2000).
5. J. Konle, H. Presting, H. Kibbel, and F. Banhart, Mater. Sci. Eng. B **89**, 160 (2002).
6. J. Stangl, T. Roch, and G. Bauer, Appl. Phys. Lett. **77**, 3953 (2000).
7. M.Ya. Valakh, V.N. Dzhagan, Z.F. Krasilnik, O.S. Litvin, D.N. Lobanov, A.V. Novikov, and V.A. Yukhimchuk, Nano Mikrosys. Tekhn. N 6, 8 (2005).
8. V.O. Yukhymchuk, A.M. Yaremko, M.Ya. Valakh, A.V. Novikov, E.V. Mozdor, P.M. Lytvyn, Z.F. Krasil-

nik, V.P. Klad'ko, V.M. Dzhagan, N. Mestres, and J. Pascual, Mater. Sci. Eng. C **23,** 1027 (2003).

9. V.P. Klad'ko, L.I. Datsenko, J. Bąk-Misiuk, S.I. Olikhovskii, V.F. Machulin, I.V. Prokopenko, V.B. Molodkin, and Z.V. Maksimenko, J. Phys. D **34**, A87 (2001).
10. O. Yefanov, V. Kladko, O. Gudymenko, V. Strelchuk, Yu. Mazur, Zh. Wang, and G. Salamo, Phys. Status Solidi A **203**, 154 (2006).
11. Yu.I. Mazur, Zh.M. Wang, G.J. Salamo, V.V. Strelchuk, V.P. Kladko, V.F. Machulin, M.Ya. Valakh, and M.O. Manasreh, J. Appl. Phys. **99**, 023517 (2006).
12. M.Ya. Valakh, V.M. Dzhagan, Z.F. Krasilnik, O.S. Lytvyn, D.N. Lobanov, O.V. Novikov, and V.O. Yukhymchuk, Ukr. Fiz. Zh. **51**, 204 (2006).
13. Z.F. Krasilnik, P.M. Lytvyn, D.N. Lobanov, N. Mestres, A.V. Novikov, J. Pascual, M.Ya. Valakh, and V.A. Yukhymchuk, Nanotechnology **13**, 81 (2002).
14. J. Groenen, R. Carles, S. Christiansen, M. Albrecht, W. Dorsch, H.P. Strunk, H. Wawra, and G. Wagner, Appl. Phys. Lett. **71**, 3856 (1997).
15. A.M. Yaremko, V.O. Yukhymchuk, M.Ya. Valakh, A.V. Novikov, V.P. Melnik, O.S. Lytvyn, D.N. Lobanov, Z.F. Krasil'nik, V.P. Klad'ko, and V.M. Dzhagan, Mater. Sci. Eng. C **25**, 565 (2005).
16. N. Usami, K. Leo, and Y. Shiraki, J. Appl. Phys. **85**, 2363 (1999).
17. R. Sauer, J. Weber, J. Stolz, E.R. Weber, K.-H. Kusters, and H. Alexander, Appl. Phys. A **36**, 1 (1985).
18. T. Roch, V. Holy, A. Hesse, J. Stangl, T. Fromherz, G. Bauer, T.H. Metzger, and S. Ferrer, Phys. Rev. B **65**, 245324 (2002).
19. D.N. Lobanov, A.V. Novikov, N.V. Vostokov, Y.N. Drozdov, and A.N. Yablonskiy, Opt. Mater. **27**, 818 (2005).

Received 15.09.10.
Translated from Ukrainian by O.I. Voitenko

ОСОБЛИВОСТІ ЗАРОДЖЕННЯ ТА УПОРЯДКУВАННЯ GeSi НАНООСТРІВЦІВ У БАГАТОШАРОВИХ СТРУКТУРАХ, СФОРМОВАНИХ НА Si ТА $Si_{1-x}Ge_x$ БУФЕРНИХ ШАРАХ

В.О. Юхимчук, М.Я. Валах, В.П. Кладько, М.В. Слободян, О.Й. Гудименко, З.Ф. Красильник, О.В. Новіков

Р е з ю м е

Методами високороздільної Х-променевої дифракції (ВРХД), комбінаційного розсіяння світла (КРС) і фотолюмінесценції (ФЛ) досліджено вплив параметрів буферного шару $Si_{1-x}Ge_x$ на просторове впорядкування самоіндукованих нанооствівців Ge у багатошарових структурах SiGe/Si, вирощених на (001)Si підкладках. Показано, що товщина та компонентний склад $Si_{1-x}Ge_x$ буферного шару впливають на латеральне впорядкування нанооствівців завдяки різній чутливості до впорядкованої модуляції деформацій на поверхні шару. Встановлено, що просторове впорядкування задається виключно латеральним впорядкуванням уже в першому періоді надґратки (НҐ). Показано, що у випадку товстих $Si_{1-x}Ge_x$ буферних шарів із значним вмістом Ge починається пластична релаксація з виникненням дислокацій невідповідності на межі поділу, а шари НҐ є когерентними до буферного шару. Комплексні дослідження структурних та оптичних характеристик дозволили розвинути методичні підходи до дослідження впорядкування нанооствівців у НҐ.